ADVANCED MATERIALS

Supporting Information

for *Adv. Mater.*, DOI: 10.1002/adma.202002361

Spider-Web-Inspired $PM_{0.3}$ Filters Based on Self-Sustained Electrostatic Nanostructured Networks

*Shichao Zhang, Hui Liu, Ning Tang, Sheng Zhou, Jianyong Yu, and Bin Ding**

Supporting Information

Spider-Web-Inspired $PM_{0.3}$ Filters Based on Self-Sustained Electrostatic Nanostructured Networks

*Shichao Zhang, Hui Liu, Ning Tang, Sheng Zhou, Jianyong Yu, Bin Ding**

Supplementary Information contains:

Experimental Section

Fabrication of nanofiber membranes. The precursor solutions were prepared by dissolving PVDF chips (M_w = 60,000, SOLVAY Shanghai Technology Park, China) and dodecyl trimethyl ammonium bromide (DTAB, >99%, Shanghai Aladdin Chemical Co., Ltd., China) in *N*,*N*-dimethylacetamide at room temperature. The PVDF concentrations in pure PVDF solutions were 12, 15, 18, and 21 wt%, while DTAB concentrations in PVDF/DTAB solutions (18 wt% PVDF) were 0.5, 1, 2, and 4 wt%, respectively. All nanofiber membranes were fabricated using a DXES-N spinning machine (SOF Nanotechnology Co., Ltd., China). The solutions were extruded out from five 10-ml syringes at feed rate of 0.1 ml h^{-1}, and the DC voltage of 30 kV was supplied to the 20-G metal needles to form jets and/or droplets to generate nanomaterials. The non-woven fabrics wrapped on the grounded metal roller (40 rpm rotating speed) were utilized to collect the nanofibrous membranes. To control membrane uniformity, the syringes were uniformly placed on the injection pump which horizontally moved backwards and forwards (speed of 150 cm min^{-1}) within a fixed distance by using a mechanical slide unit. And, electric shield devices on the needles were employed to ensure that the jet/droplets flew forward, thus the nanofibers could be uniformly deposited during the quadrature motion process caused by the synchronous movement of the stainless roller and mechanical slide unit.

Characterization. The precursor solution properties and charge densities of the liquids during electro-spraying-netting were measured using the equipment and methods depicted in our previous work (*20*). Phase translation observation of PVDF solutions was performed using an Olympus BH2-UMA microscope equipped with IS Capture image program (Supplementary Methods). The microscopic architectures (such as morphologies and pore structures) and chemical structures (for example, crystalline phase) of the resultant nanomaterials were characterized by SEM (Hitachi S-4800, the samples were pre-coated with carbon for 3 min), capillary flow porometer (CFP-1100AI), BET surface area analyzer (ASAP2020), FT-IR

spectroscopy (Nicolet 8700), and XRD (D/Max-2550 PC). The base weight and thickness of the membranes were measured using a Mettler Toledo Micro balance (AT-20, readability of 2 μg) and a Labthink thickness gauge (CHYC2), respectively. The mechanical properties, piezoelectric properties, and surface potentials were collected using a tensile tester (XQ-1C), LSV (OFV-3001-SF6), and non-contacting electrostatic probe (VM54XQS). The transmittance spectrum of the SWING air filters was determined by a PG 2000+ spectrometer (400–800 nm). The removal efficiency and air resistance of the SWING filters for PM filtration were measured using a filter tester (LZC-H, Supplementary Methods). A clinical isolate of *Staphylococcus aureus* (*S. aureus*, SA1004) obtained from Ruby Memorial Hospital (Morgantown, WV, US) was used to generate *S. aureus*–containing aerosols (0.3–5 μm) to evaluate the bioprotective activity of the filters. PM purification tests were carried out using a self-designed equipment used in our previous work (*5*).

Supplementary Methods

Measurement of the charge density of the liquids

The typical method of "mesh target" widely used in conventional electrospray technology, was ulitized to measure the charge density of the liquids during electro-spraying-netting process. The receiver substrate and the ground terminal of the high-voltage DC power supply were connected together through a high precision multimeter (Fluke F15B+) which can measure the current induced by the flying charged jet/droplets. During a certain time (t), the total charge (e) can be obtained by: $e = I \times t$, where I represents the average current value. And, we calculated the mass (m) of the liquid in the same period by the formula: $m = M/c$, in which M is the mass of the membrane and c is the PVDF concentration. Here, the current was recorded once a minute, and at least 5 parallel tests were carried out to measure the charge density (e/m) of the liquid for each kind of samples.

Characterization of the phase separation of PVDF solutions

We performed the optical microscopy measurement using an Olympus BH2-UMA microscope equipped with IS Capture image program. ~0.05 ml PVDF solution was dropped on the concave center of a quartz slide, and its micro-morphology evolution history was recorded by IS Capture. The Photoshop CS6 image software was utilized to quantify the gray levels of the resultant micrographs. All process parameters, such as light intensity, ambient temperature, etc. were set unchanged. The gray levels of these micrographs are proportional to the transmitted light intensity of the solutions, and it takes values from 0 to 255. The relative light transmittance (RT) of PVDF solutions can be defined by: $RT = G_t / G_0$, in which the G_t and G_0 are the gray level of the micrograph of the studied solution at time t and initial time t_0, respectively. Thus, the RT deviation (RT_D) can be calculated by: $RT_D = G_{tD} / G_t$, where the G_{tD} is deviation of the gray level of the micrograph of the sample at time t. Because the RT value of the solution decreased due to solvent evaporation, we choose the change of RT as an indicator to characterize the solidification speed of the solutions. The RT deviation indicates the homogeneity of the studied solutions, and we regard it as the speed of phase separation of various PVDF solutions.

Coverage rate of the networks in the membranes

The coverage rate of the networks that supported by conventional electrospun fibers in PVDF membranes was defined as the area ratio of the integral ‘‘mesh structure’’ to the whole membranes; and measured by a “grid method” from a series of SEM images independently. At least 10 SEM images were taken and analyzed carefully, then the average value was obtained.

Crystallinity of the PVDF nanofiber membranes

Based on the FTIR spectra, we further calculated the relative content of β polymorphs using the following equation: $C(\beta) = A_\beta/(1.26A_\alpha+A_\beta)$,where A_α and A_β are the transmittance bands at 763 and 840 cm^{-1}, respectively.

Filtration measurement of the air filters

We measured the filtration performance of the air filters using a LZC-H filter tester (Huada Filter Technology Co., Ltd.). The nanofiber membranes (area of 100 cm^2) were clamped by the filter holder. Then, 0.3–0.5 or 20 million charge neutralized solid NaCl or oil DEHS aerosol particles, that generated using the atomizer, were delivered through the testing filter at a designed airflow velocity (ranging from 5.33 to 20 cm s^{-1}) by the air pump. These PMs had a mass mean diameter range of 0.1–10 μm and a geometric standard deviation <1.86. The removal efficiencies of air filters were tested using two laser particle counters, and their pressure drops were measured by two electronic pressure transducers. A minimum of five regions with area of 100 cm^2 were measured for each kind of filter membranes (each sample size of 65 × 25 cm^2) to ensure the representativeness and reliability. Unless otherwise indicated, the testing airflow velocity was designed as 5.33 cm s^{-1}, in considering that it is usually regarded as the industrial testing standard according to the European standard (EN779: 2012) and USA standard (IEST-RP-CC52.2-2007) for air filters. And, most of the global manufacturer companies for air filters, like Hollingsworth & Vose, have employed this velocity as the main testing condition for the filtration materials. Moreover, scanning the literature sources about the air filtration, most of them selected the airflow velocity of 5.33 cm s^{-1} to test the filter performances. In addition, the quality factor (*QF*), as a trade-off indicator to evaluate the filtration capacity of air filters based on their removal efficiency and air resistance, can be defined by the formula: $QF = -ln(1 - \eta)/\Delta p$, in which the η is the removal efficiency and the Δp is the pressure drop.

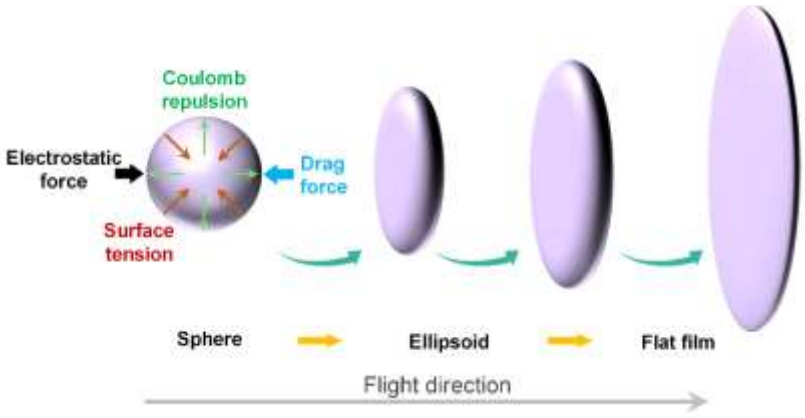

Figure S1. Forces acting on the charged droplet and its deformations during the fast flight in electrostatic field.

After ejection, the charged droplets flew with a high speed toward the receiver, powered by the electric force, and underwent a rapid geometric deformation from 'sphere' (several micrometers or less) to 'flat plate' (dozens even hundreds of micrometers) due to the synergetic effect from external forces. Thus this rapid (within millseconds or less) but significant expansion process resulted in the aligning of molecule chains in the nanowires of the networks in a plane perpendicular to the flying direction. Besides the nanoscale diameters (<1/10 of conventional electrospun nanofibers) and ion-dipole interaction, the rapid solidification without residual solvent greatly suppressed the disorientation kinetics of aligned PVDF molecules and facilitated the formation of β-phase crystal in PVDF nanowires.

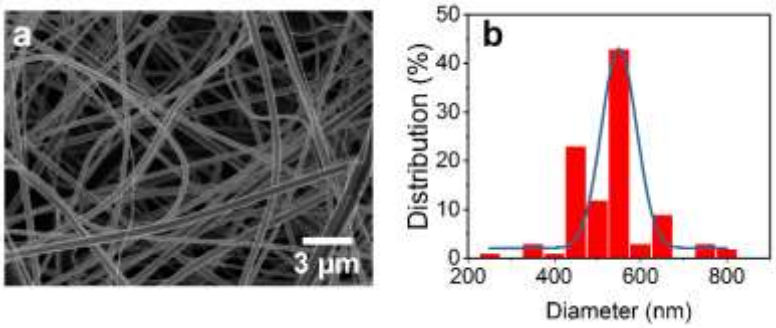

Figure S2. (a) SEM image and (b) fiber diameter distribution of the PVDF nanofibers.

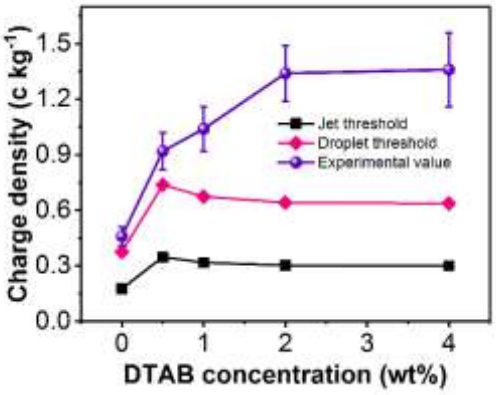

Figure S3. Charge density of the fluids obtained from PVDF/DTAB solutions with different DTAB concentrations. The thresholds mean the theoretically required charge densities of the liquids to form jets and droplets, and can be calculated according to the numerical model for Taylor cone ejection.

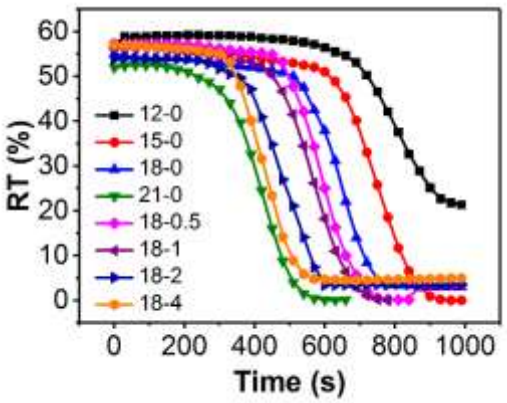

Figure S4. Relative light transmittance (RT) as a function of evaporation time for various solutions. X-Y solution, X and Y are PVDF and DTAB concentrations (wt%), respectively.

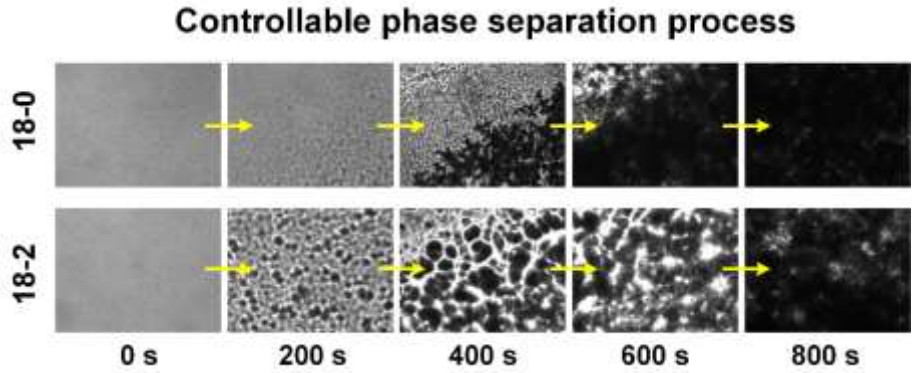

Figure S5. Snapshots of the evolving phase separation of PVDF and PVDF/DTAB solutions at time t = 0, 200, 400, 600, and 800 s (from left to right).

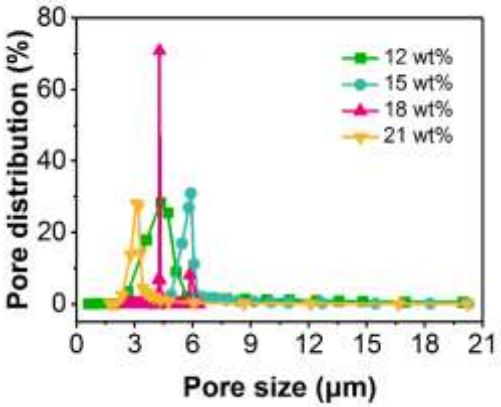

Figure S6. Pore size distribution of the nanofiber membranes fabricated from solutions with different PVDF concentrations.

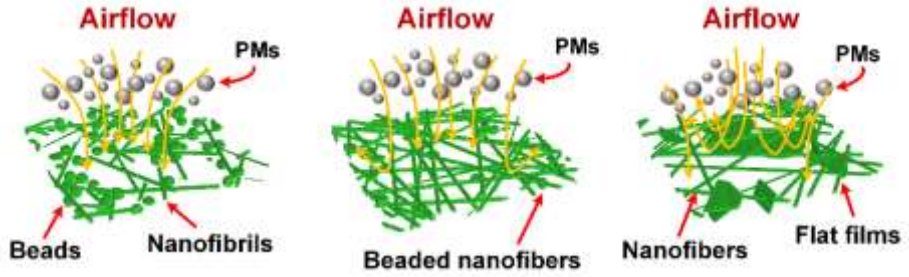

Figure S7. Schematic showing the PM filtration processes using different microparticle/nanofibril, beaded nanofiber, and nanofiber/film membranes.

In contrast to the hydrophobic PVDF nanofibers (water contact angle (WCA) of ~130°), the NF-nets obtained from solutions with 2 wt% DTAB were hydrophilic and showed WCA of ~12°. We mainly attributed this result to the presence of DTAB on fiber surfaces and the capillary effect of high porosity of the NF-nets. Obviously, the DTAB was remained both inside and at the surface of the NF-nets, and probably most of them were spread over the fiber surfaces, because the hydrophobic ends of DTAB preferred to embed in the hydrophobic PVDF matrices due to similar polarity while exposing their hydrophilic groups outside. The PM particles have complicated compositions including inorganic matter (such as SiO_2, SO_4^{2-}, and NO_3^-) and organic matter (such as organic and elemental carbon); and abundant polar functional groups such as C–O, C=O, and C–N are present at the outer surface of the PM particles. Therefore, the exposing hydrophilic group ($-N^+(CH_3)_3Br^-$) of the DTAB on the NF-nets can interact with the surface functional groups of PMs, probably providing the ionic sites for air filtration.

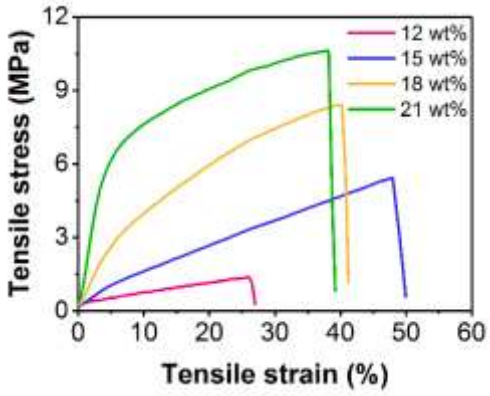

Figure S8. Tensile stress-strain curves of the nanofiber membranes fabricated from solutions with different PVDF concentrations.

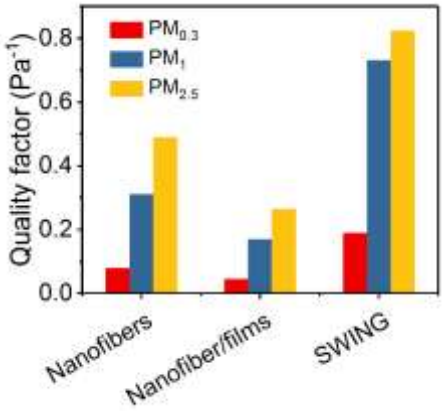

Figure S9. Quality factor of the PVDF nanofiber, nanofiber/film, and SWING air filters for $PM_{0.3}$, PM_1, and $PM_{2.5}$ removal. Airflow velocity, 5.33 cm s^{-1}.

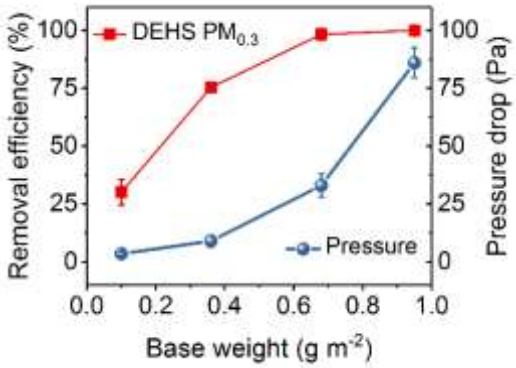

Figure S10. DEHS $PM_{0.3}$ removal efficiencies and pressure drops of the SWING filters with various base weights. Besides excellent removal capability for rigid NaCl PMs, the SWING filters with base weight of ~0.95 g m^{-2} achieved 99.983% efficiency for capturing oil based DEHS $PM_{0.3}$ while maintaining a pressure drop of 86 Pa.

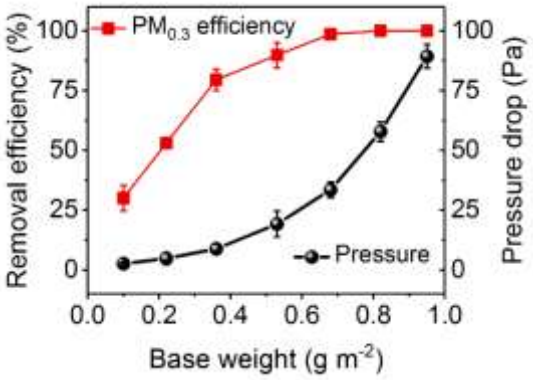

Figure S11. NaCl $PM_{0.3}$ removal efficiencies and pressure drops of the SWING filters with various base weights (PM number concentration of 20 million). With increasing the PM concentration from 0.5 to 20 million, the SWING filters exhibited a slightly decreased efficiency for $PM_{0.3}$ removal, for example, from 99.923% to 99.913% for 0.82 g m^{-2} filters and from 99.995% to 99.991% for 0.95 g m^{-2} filters (Figure 4b). This steady removal capacity could be attributed to the unique combination of sieving and electrostatic adhesion manner and airflow slip-effect originating from nanostructured networks.

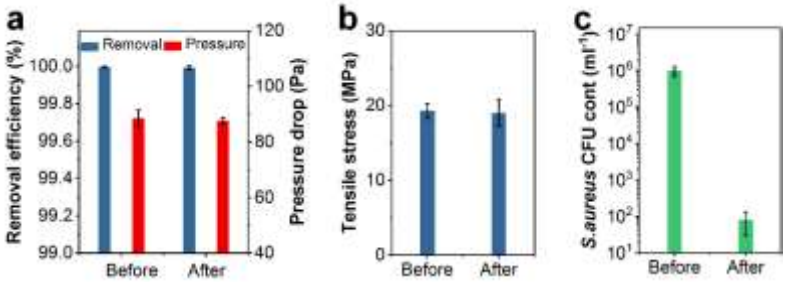

Figure S12. (a) $PM_{0.3}$ removal efficiency and pressure drop, (b) tensile stress, and (c) *S. aureus* killing performance of the SWING air filters before and after exposing UV radiation for 24 h.

Table S1. Effect of polymer systems on the charge state of fluids during electro-spraying-netting process.

Polymer system	12-0	15-0	18-0	21-0	18-0.5	18-1	18-2	18-4
ε (F m^{-1})	37.8*8.85*10^–12							
γ (mN m^{-1})	35	33.4	32.2	28.2	29.9	27.5	25.1	22.5
ρ (kg m^{-3})	1044	1068	1092	1116	1092	1092	1092	1092
η (cps)	590	1220	2650	5260	4530	5550	5800	5950

K (μS cm^{-1})	4.55	3.79	3.01	2.32	798	1318	1845	3450
Q (ml h^{-1})	0.1							
D (m)	1.499* 10^–5	1.962* 10^–5	2.617* 10^–5	3.507* 10^–5	1.628* 10^–5	1.68*1 0^–5	1.685* 10^–5	1.632*10 ^–5
Jc (c kg^{-1})	0.4453	0.2839	0.177	0.1045	0.3476	0.3179	0.3024	0.3004
Dc (c kg^{-1})	0.9445	0.6022	0.3754	0.2216	0.7373	0.6745	0.6415	0.6372

Table S2. The removal efficiencies, pressure drops, and *QF* values of various air filters.

Air filters	**Removal efficiency (%)**			**Pressure drop (Pa)**	***QF* (Pa^{-1})**		
--	$PM_{0.3}$	PM_1	$PM_{2.5}$	--	$PM_{0.3}$	PM_1	$PM_{2.5}$
Nanofibers	35.2398	81.8651	93.2213	5.5	0.079	0.311	0.489
Nanofiber/films	39.5326	85.6652	95.2234	11.5	0.044	0.169	0.264
SWING	65.2235	98.3325	99.0035	5.6	0.189	0.731	0.823

Table S3. *Knudsen* numbers and flow regimes dependent on different ranges of fiber diameter under normal condition.

Fiber diameter (*d*)	**Knudsen number (*Kn*)**	**Flow regimes**
$d > 132$ μm	$Kn < 0.001$	Continuum flow
528 nm $< d <$ 132 μm	$0.001 < Kn < 0.25$	Slip flow
13.2 nm $< d <$ 528 nm	$0.25 < Kn < 10$	Transition flow
$d <$ 13.2 nm	$Kn > 10$	Free molecular flow

Supplementary Derivation

Ejection models of the charged fluids on Taylor cone apex.

In this work, we chose the apex diameter of the Taylor cone at the maximum curvature as the diameters of the ejected jet/droplets, and these diameter can be calculated by: $D = 1.46Q^{0.44}\varepsilon^{0.12}\eta^{0.32}K^{-0.12}\gamma^{-0.32}$. In considering that the gravity of the liquid is negligible due to its tiny weight, the ejection on Taylor cone can only occur on the basic prerequisite of the following equation: $F_e > F_\gamma$.

For jet ejection, a cylindrical fluid is assumed to generate from Taylor cone, thus, the hydrostatic pressure F_γ was: $F_\gamma = \gamma / R$. And, the Coulomb repulsion F_e was be expressed as: $F_e = \frac{e^2}{8\varepsilon\pi^2 R^2 l^2}$.

For droplet ejection, a sphere fluid is assumed to generate from the Taylor cone, the hydrostatic pressure F_γ caused by the surface tension was: $F_\gamma = 2\gamma / R$. And, its Coulomb repulsion F_e was: $F_e = \frac{e^2}{32\varepsilon\pi^2 R^4}$.

Therefore, based on solving the simultaneous equations, the critical conditions of these two ejection modes of jet and droplet were obtained.